Characterization of the effect of in-process annealing using a novel print head assembly on the ultimate tensile strength & toughness of Fused Filament Fabrication (FFF) parts

Parimal Patel, Rhugdhrivya Rane, Manjarik Mrinal, Vishnu Ganesan, Robert Taylor & Ankur Jain

Published online: 25 Jul 2022.

Submit your article to this journal ⬈

Article views: 113

View related articles ⬈

View Crossmark data ⬈

Taylor & Francis
Taylor & Francis Group

Check for updates

Characterization of the effect of in-process annealing using a novel print head assembly on the ultimate tensile strength & toughness of Fused Filament Fabrication (FFF) parts

Parimal Patel*, Rhugdhrivya Rane*, Manjarik Mrinal, Vishnu Ganesan, Robert Taylor and Ankur Jain

Department of Mechanical and Aerospace Engineering, University of Texas at Arlington, Arlington, TX, USA

ABSTRACT

Improving the quality of parts printed using Fused Filament Fabrication (FFF) is of critical importance in a number of engineering applications. Providing additional thermal energy during printing by external means, or by an integrated heater has been investigated in the past to prolong the cooling curve, and therefore, ensure good adhesion with adjacent filaments. This work presents a modified heater block assembly to apply in-process thermal load during the upright printing of a Polylactic Acid (PLA) part. The design overcomes key shortcomings of past work and, in particular, addresses effective printing of thin, tall structures, where filament adhesion between layers is of particular importance. Cross-section imaging and tensile testing is combined with a comprehensive statistical design of experiments in order to fully understand the impact of process parameters on improved mechanical strength of printed parts. This work contributes towards improved properties and performance of realistic and practical FFF-printed parts.

1. Introduction

There has been much recent evolution in manufacturing techniques for fabricating complex parts. Additive manufacturing (AM) is one such set of techniques that has gained popularity due to its capability to fabricate parts that would otherwise be difficult to do with conventional methods (Dimitrov, Schreve, and De Beer 2006; Zein et al. 2002). AM allows customised and sustainable manufacturing with expanded design flexibility and ease of accessibility (Bromberger and Richard 2017; Ligon et al. 2017). Unlike conventional methods such as mold-manufacturing, AM prints the part in a bottoms-up approach (Hod Lipson 2013; Patel et al. 2019; Dhal 2018). According to the ASTM F42 committee, AM processes have been divided into seven categories to standardise terminology. Fused Filament Fabrication (FFF), which belongs to the Material Extrusion category (ASTM F42), is one of the most common AM techniques in the terms of the number of parts fabricated and printers worldwide (Turner, Strong, and Gold 2014). In FFF, a Computer-Aided Design (CAD) model is used to manufacture the final part by depositing one hot extrudate onto the another. FFF can be differentiated from the most AM techniques because it does not use an energy source that rasters over a powder bed, selectively

bonding the powder due to the melting and solidifying while fabricating the final geometry (Pham and Gault 1998; Kruth, Leu, and Nakagawa 1998; Wong and Hernandez 2012; Zhang, Liao, and Coddet 2012; Tolochko et al. 2003). As seen in Figure 1, in FFF systems, a thermoplastic filament is heated above its glass transition temperature to form a polymer melt which is dispensed through a heated liquefier onto a heated build platform (Pham and Gault 1998; Kruth, Leu, and Nakagawa 1998; Gibson, Rosen, and Stucker 2015). With the help of a gantry, the print nozzle is moved in the *xy*-plane as it deposits the material whereas either the bed or the nozzle is moved in the *z*-direction for the out of the plane movement. However, parts printed using FFF are known to offer poor mechanical properties (Osborn et al. 2015; Ahn et al. 2002; Bellini and Güçeri 2003) compared to the baseline material or injection molded counterparts.

Previous research has studied the inter-laminar failure of the parts under various loading conditions including tensile (Cole et al. 2016), compressive (Percoco, Lavecchia, and Galantucci 2012; Sood, Ohdar, and Mahapatra 2012), fatigue (Domingo-Espin et al. 2018; Gomez-Gras et al. 2018; Puigoriol-Forcada et al. 2018) and torsion (Rodríguez, Thomas, and Renaud 2001). These studies

---

CONTACT Ankur Jain ✉ jaina@uta.edu 🔲 Department of Mechanical and Aerospace Engineering, University of Texas at Arlington, Arlington, TX 76019, USA
*These authors contributed equally.
This article has been corrected with minor changes. These changes do not impact the academic content of the article.
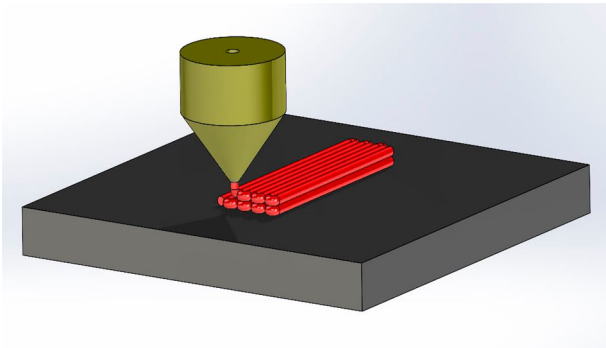
Figure 1. Schematic of the filament deposition process in FFF.

reinforce the idea that the reduced mechanical properties are a function of the inter-laminar bonding between the layers. When the polymer melt is deposited, the adjacent filament rasters merge into each other resulting in the formation of the inter-laminar bonds or necks. However, as the temperature of the melt approaches the glass transition temperature, the polymer melt becomes highly viscous, which slows down and eventually stops the neck formation process (Duty et al. 2018; Costa, Duarte, and Covas 2017). The thermally-driven neck formation and growth process is critical to inter-laminar bonds, and thus the mechanical strength of printed parts (Ahn et al. 2002). It has also been observed that the print parameters such as print temperature (Lanzotti et al. 2008), air gap (Rodríguez, Thomas, and Renaud 2001) and print orientation (Ziemian, Okwara, and Ziemian 2015) affect the mechanical properties of the FFF parts. Porosity is an intrinsic defect seen in FFF parts because the rounded features generated by the circular nozzles lead to imperfectly stacked layers (Rodriguez, Thomas, and Renaud 2000). This further leads to the formation of long void gaps between the two adjacently deposited polymer beads, accentuating the premature failure of the FFF parts.

Various papers have highlighted the importance of temperature and heat transfer in determining the properties of the FFF parts through various experiments. It has been shown that the complex temperature distribution around the deposited polymer melt combined with the heat transfer between the adjacent filaments determines the quality of bond (Costa, Duarte, and Covas 2017). Furthermore, work has been done on the different in-process and post-process techniques to accentuate the neck growth in FFF parts. Previous work on post-process thermal annealing has shown that increasing the inter-laminar bonding by heating the part well beyond its glass transition temperature results in a significant increase in the mechanical strength of the parts. This method does lead to a substantial increase in strength, but geometric accuracy of

the part is compromised and application of a post-process thermal load increases the total build-time of the final part (Rane et al. 2020; Tamburrino et al. 2021). Post-process annealing can take up a significant amount of time. Other approaches have been studied to provide an external heating source to facilitate the inter-laminar bonding. For example, microwave heating has been used to raise the local temperature during the fabrication of FFF parts (Sweeney et al. 2017). However, these approaches utilise complex and expensive additional equipment which complicates the FFF process. Another study was done by Ravoori et al., where a rectangular metal block was attached to the nozzle assembly to apply an in-process thermal load, thus enabling increase in neck growth (Ravoori et al. 2019). This provided a comparatively simple and a cost-effective technique to increase the inter-laminar bonding by the in-process heating. Also, the previous studies have shown that the inter-laminar bonds are weakest along the out-of-plane or the z-direction due to the reduced reptation and neck formation when a hot polymer melt is extruded onto a layer that is already cold (Keleş, Blevins, and Bowman 2017; Zaldivar et al. 2017; Costa, Ferreira da Silva, and Sousa Carneiro 2019). In the work done by Ravoori et al, the tensile coupons printed were laid flat onto the bed, and thus, the primary neck growth process occurred between adjacent beads on the same layer, rather than between layers. The issue of the layer bonding manifests itself in the printing of a thin and tall structure, such as upright printed tall parts in a small radio-controlled (RC) aircraft design, and may be the reason of these parts failing due to reduced z-strength (Skawiński and Goetzendorf-Grabowski 2019; Taylor et al. 2020; Kopecki, Mazurek, and Święch 2020; Luo et al. 2021; Ahn et al. 2002). Thus, it is desirable to take these issues into account, evaluate what parameters affect the necessary in-process thermal load in improving the layer bonding, and provide a solution to the reduced mechanical properties of FFF parts, especially in the z-direction.

In the current work, a modified heater block assembly has been designed to apply an in-process thermal load during the upright printing of a Polylactic Acid (PLA) part. A heater block is designed with a circular block integrated into the heated liquefier. Two factors, namely block thickness and nozzle height are studied with 3 levels to statistically investigate the effect of these parameters on the necessary thermal load to improve the layer bonding in the printing of tall and slender parts. A design of experiments (DOE) is performed using a two-way full factorial analysis to study and characterise the ultimate tensile strength (UTS)

and obtain a statistical model. Analysis of Variance (ANOVA) is conducted to test the significance of each factor on the increase in the UTS in the z-direction and to find the optimum value from the different combinations. Image processing is used to analyze the change in the characteristic of the long voids seen between the adjacent rasters as well as the change in the shape of the void area.

2. Experiments

For the experiments, the parts were printed using 1.75 mm diameter PLA filament (Hatchbox 3D, Pomona, CA, USA). Dogbone-shaped tensile test coupons were printed using a modified design of the ASTM D638-02a standards as shown in Figure 2 (Rane 2018; "Compass" 2022; Patel 2018). The tensile test coupons were designed on SOLIDWORKS 2016 (Dassault Systems, Waltham, MA, USA) and converted to a G-Code using Simplify3D (Simplify3D, Blue Ash, Ohio, USA) software. Figure 3 shows the experimental setup consisting of a Creality Ender 3 Pro printer with the attached modified heater block assembly with 0.4 mm nozzle. The print parameters used are specified in Table 1. The infill percentage for the coupons was kept at 100% with no perimeter shells. The use of a different material may need a recalibration of some of the print parameters. Previous studies had used a print setting which provided the parts with a considerably low reference value as compared with those obtained by the current settings leading to an inaccurate and inflated depiction of the factor effects. These print settings were used as they provided the best results in terms of print quality, strength, and reduced print times. The temperature of the heater block disc and nozzle are the same at 200°C since they are connected to each other. It is the same temperature as the extrusion temperature set in the Gcode. The dog bone samples were printed with their longest dimension parallel to the build direction (z-direction). This was done to achieve an accurate representation of the weak inter-laminar bonds between the two adjacent layers and therefore provide results for an increase in the UTS for the weakest inter-laminar bonds. The infill raster angle was kept at 0° to obtain a maximum inter-laminar bond area.

The circular aluminum heater block discs were 50 mm in radius and had three levels of thickness: 2, 5, and 10 mm. Aluminum was used because of low weight and ease of machining. The nozzle height from the block was adjusted to three levels: 1, 1.5, and 2 mm. The nozzle height is defined as a distance between the nozzle tip and bottom of the heater block. Print speed of 60 mm/s is still attainable with the heater block

discs due to the lightweight aluminum. A cooling fan with a duct was provided for a localised cooling above the heated liquefier region, as seen in Figure 3. Localised cooling is necessary because preliminary tests with the fan without localised cooling showed that heat generated due to the block travels upwards via conduction, leading to softening of the filament in the upper sections of the extrusion chamber, which ultimately caused print failure after a few layers. While the cooling fan at the cold end is a normal attachment on an FFF printer, localised cooling through a duct is a critical part of this experiment setup, considering the additional thermal load being generated through the heater block.

Each part was printed separately to avoid any compounding error and provide replications for the different factor levels. The parts were then tested under tensile loading using a Shimadzu Tensile Testing machine. To apply the tensile load, a displacement control of 5 mm/min was applied on the specimens using a 10 kN Load cell. The load vs stroke data from tensile tests was converted to stress versus strain by dividing with the appropriate values of the area and length, respectively. The maximum value of the stress of each specimen was considered as the ultimate tensile stress (UTS) whereas the area under the curve was calculated to obtain the toughness (strain energy) of the parts. The stiffness of the parts was calculated in accordance with the ASTM Standard D638 by providing appropriate toe compensation and assuming Hookean behaviour in the lower sections of the Stress–Strain curve.

The experiments and analysis were conducted using a full factor DOE for the two response variables: Increase in UTS and Increase in Toughness. To obtain a comprehensive statistical model and the factor level effects, three levels of nozzle height and plate thickness were chosen as summarised in Table 2. The two-way full factorial DOE runs for each combination of factors are mentioned in Table 2. Thus, the experimental design included a total of nine treatment combinations with five replications for each treatment. To avoid the systematic biases, the treatments were performed in a randomised order. Each part was printed separately on the Creality Ender 3 with each part taking about 68 min to print. After each print, the brim (skirt) around the specimen was removed carefully with no further post-processing on the specimen. After completing all the treatments, the parts were tested under a tensile load to obtain the ultimate tensile strength and toughness. The reference values were obtained by printing 4 specimens with the same G-code as the treatments, using the stock heater block assembly as provided with the
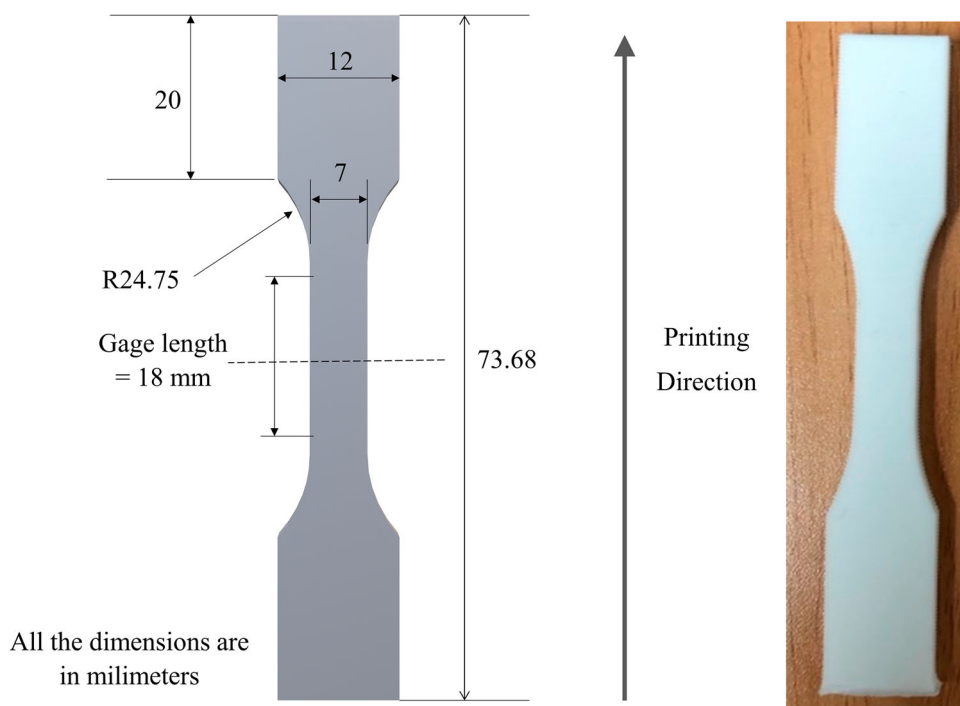
Figure 2. Dimensions of modified ASTM D638-02a specimen and an actual printed specimen.

Creality Ender 3. The increase in the tensile strength and toughness are obtained by subtracting the values obtained for the control specimens from those of the treatment combinations. The values of stress, strain and toughness were calculated using MATLAB and the statistical analysis was performed using SAS (SAS Institute Inc; Cary, NC).

3. Results

In the following discussion, the DOE assumptions have been verified and the appropriate statistical model along with the ANOVA have been stated.

3.1. Raw increase in the strength and strain energy due to the nozzle height and plate thickness

3.1.1. Raw increase in the UTS

Experimental data presented in Figure 4 clearly shows an increase in ultimate tensile strength in the treatment combinations obtained by subtracting the average value for control specimens from those of the treatment

Table 1. Print parameters used in this work.

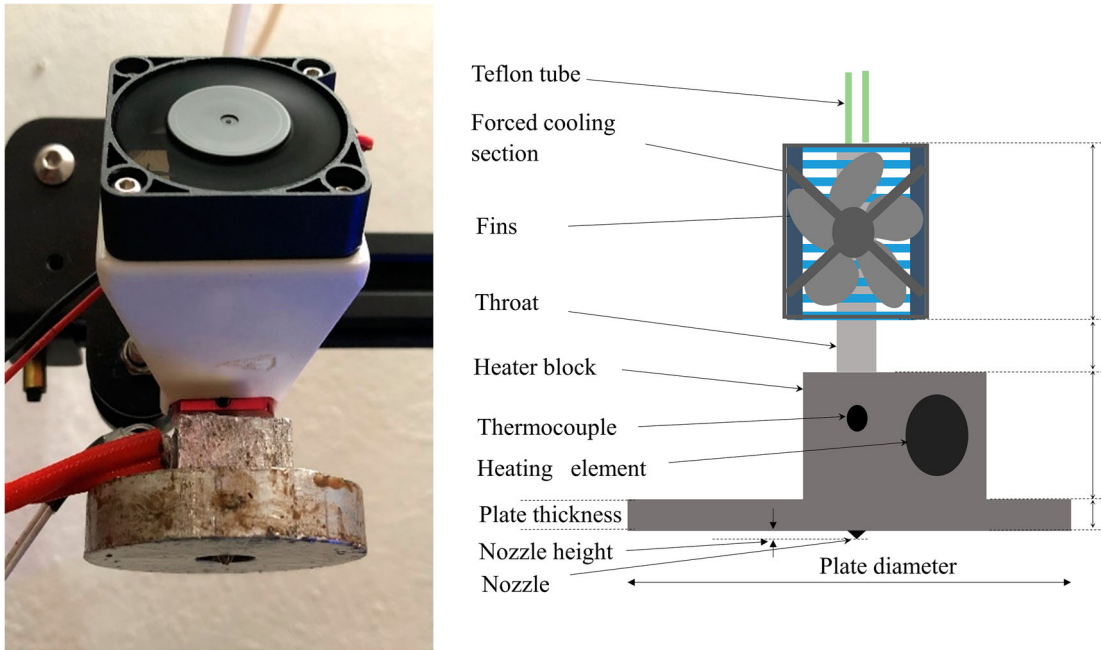| Parameter	Print speed	Layer height	Infill	Print temperature	Bed temperature
Value	60 mm/s	0.2 mm	100%	200℃	60℃

combinations with respect to the nozzle height. The dots in the figure represent these values. Figure 4 shows that as the nozzle height increases from 1 mm to 2 mm, the average ultimate tensile strength reduces somewhat. This is likely because as the nozzle height approaches 2 mm, the top layer is exposed to a lower temperature field as compared to that when the nozzle height is kept at 1 mm. These differences in the temperature profiles with the changes in the nozzle height affect the bonding between the layers. Previous studies have shown that when the temperature of the previous layer is maintained at a higher level an increase in the strength is obtained due to the better neck formation (Sweeney et al. 2017). This holds true for the current study; we see that the average increase in the ultimate tensile strength of the parts falls from 23.3 MPa to 16.2 MPa as we increase the nozzle height from 1 mm to 2 mm.

In contrast with the impact of nozzle height, however, no trend or notable difference is seen in the measured strength with plate thickness, as shown in Figure 5. The average increase in the strength is seen to be maximum for the 2 mm plate thickness, followed by 10 and 5 mm plate thicknesses, but the difference is relatively small.

Figure 6 presents boxplots for the distribution of increase in the UTS. Figure 6 shows that the nozzle height has a dominant effect on the increase in ultimate tensile strength of the parts as compared to the plate thickness. A general upward trend is noticed as the nozzle

Figure 3. Print head assembly.

height is varied from 2 mm to 1 mm. No such trend can be concluded for the effect of the plate thickness on the increase in ultimate tensile strength of the parts.

3.1.2. Raw increase in toughness (strain energy)

From Figure 7, it is seen that the effect of nozzle height on toughness is similar to the effect on UTS. As the nozzle height goes from 1 mm to 2 mm, a consistent fall in the strain energy is seen. The average increase in the toughness of the parts falls by more than 50% (2159 KPa to 1029 KPa) as the nozzle height increases from 1 mm to 2 mm. The increase in toughness can be correlated to reptation across the interfaces which is influenced by the exposure temperature and time duration. For a nozzle height of 1 mm, the top layers are exposed to a much greater temperature as compared to the nozzle height of 2 mm, thus leading to a significant fall in toughness with the increase in nozzle height. At 1 mm nozzle height, there is greater reptation and intermingling of the polymer chain leading to an enhanced toughness.
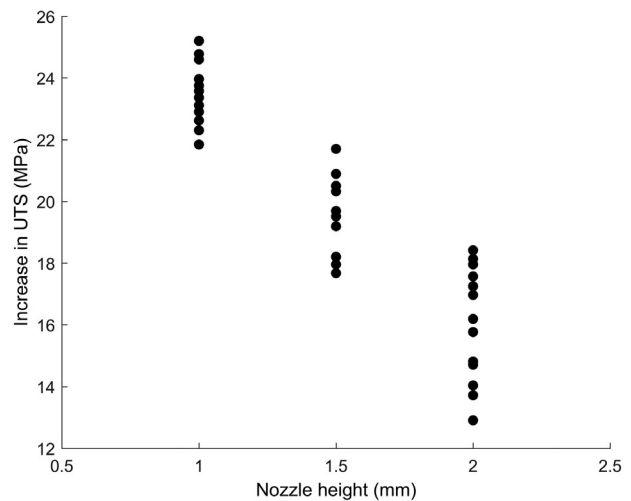
Figure 8 presents the effect of plate thickness on raw increase in toughness. A general upward trend in the average toughness is found as the plate thickness

increases, with an increase from 1225 kPa to 1742 kPa between 2 and 10 mm plate thickness. This can be attributed to the fact that for a larger plate, the layers are exposed to a higher value of temperature for a longer time duration, but further investigation such as numerical simulations may be needed to comprehensively test this hypothesis.

The boxplots in Figure 9 show that the increase in the toughness has a larger spread for the plate thickness as compared to the nozzle height showing a dominant effect of the nozzle height. Also, a positive correlation is seen between the increase in the plate thickness

Table 2. Nozzle height and plate thickness levels for the design of experiments.

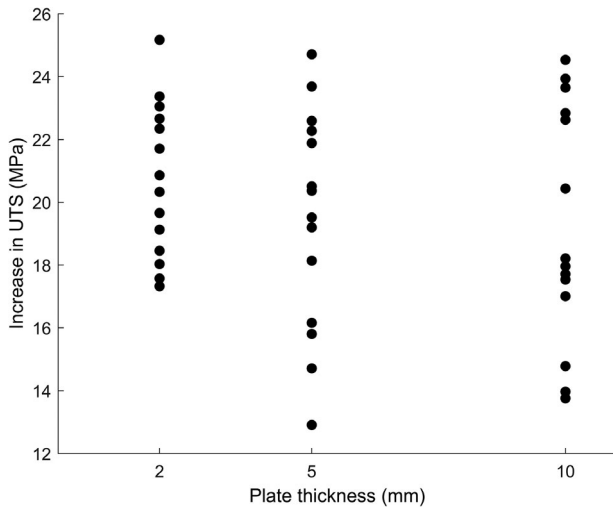| Levels	Nozzle height (mm)	Plate thickness (mm)
1	1	2
2	1.5	5
3	2	10

Figure 4. Plot showing the raw increase in the strength with the nozzle height.

Figure 5. Plot showing the raw increase in the strength with the plate thickness.

Figure 7. Plot showing the raw increase in the toughness with the nozzle height.

with the increase in the toughness whereas a negative correlation between the increase in the nozzle height and increase in the toughness is seen.
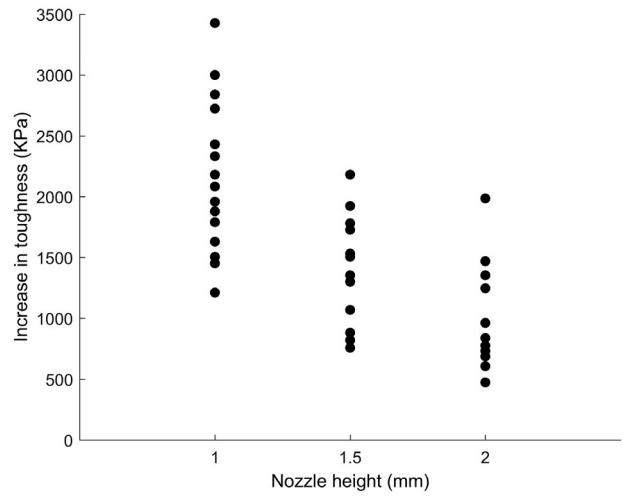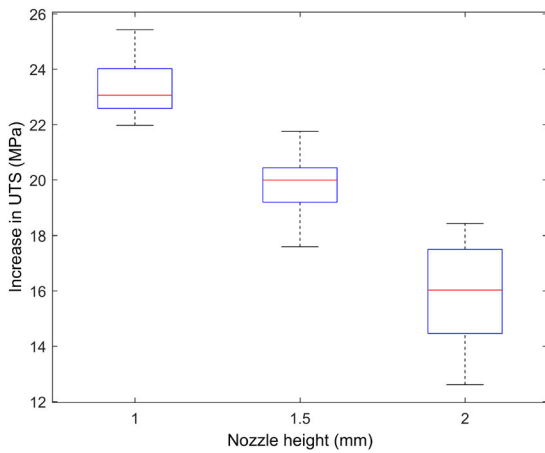
3.2. Two-way fixed effects model and verification of assumptions

In the current study for both response variables, the two-factor full interaction model is given as

$$Y_{ijt} = \mu + \alpha_i + \beta_j + (\alpha\beta)_{ij} + \varepsilon_{ijt} \tag{1}$$

Where μ is the overall mean, α_i and β_j represent the main effects due to the nozzle height and plate thickness. Further, $(\alpha\beta)_{ij}e$ and ε_{ijt} are represent the interaction effects and the associated error term.

Here we assume that the model has unknown fixed effects subjected to the following restrictions: $\sum_i (\alpha)_i = 0$, $\sum_j (\beta)_j = 0$, $\sum_i (\alpha\beta)_{ij} = 0$ and $\sum_j (\alpha\beta)_{ij} = 0$. Also, it is

assumed that the error term in the ANOVA model, ε_{ijt} is normally distributed with a constant variance and mutually independent errors. The assumption of the normally distributed residuals is tested by visually inspecting the Normal Probability Plot (NPP) for both responses, as shown in Figure 10. It is seen that both plots have some sampling variations, but there do not exist any heavy tails or other serious departure from normality. Therefore, the assumption of the normality is satisfied for both response variables (Dean and Springer 2017). As a result, a transformation does not need to be applied to the data, and the linear model shown in Equation 1 is reasonable.

In order to verify the assumption of a constant variance, the residuals are plotted as a function of the fitted values (estimated means, $\widehat{y}$) as shown in Figure 11. Figure 11 shows that there are no collocated residuals for both response variables (average increase
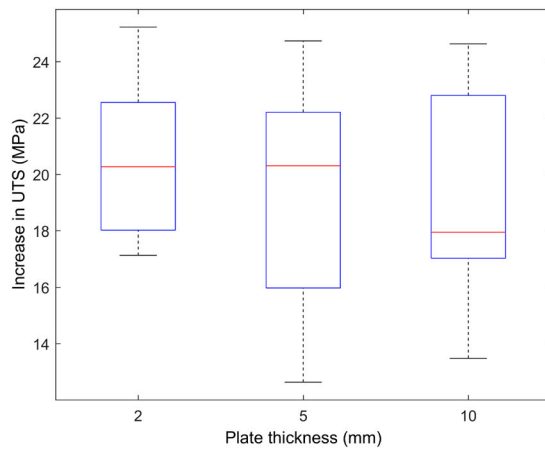
Figure 6. Boxplot showing the variance in the distribution of the increase in the UTS for the different nozzle heights and plate thicknesses.
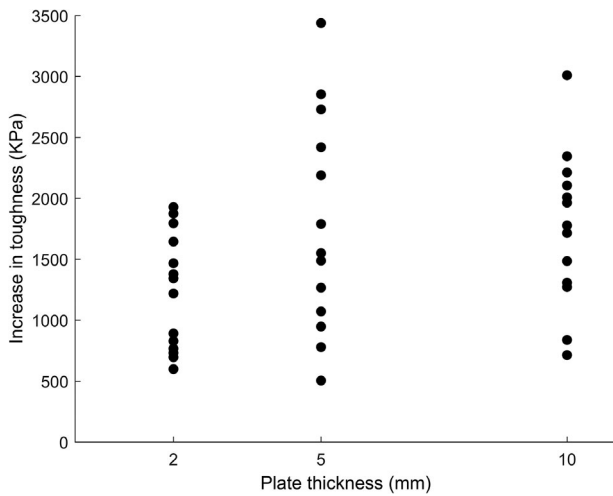
Figure 8. Plot showing the raw increase in the toughness with a plate thickness.

in the UTS and average increase in the toughness), and the scatter of points are randomly distributed with somewhat equal spread. Therefore, the assumption of constant variance is reasonable.

3.3. ANOVA and factor interactions

This section discusses the ANOVA and factor interactions from the DOE. First, the increases in UTS and toughness are discussed. Next, pairwise comparisons are made for the response variables. Finally, an optimised design of the heater block assembly is presented.

3.3.1. Increase in UTS

From the interaction plots shown in Figure 12, three distinct lines are seen, which show that the main effects for the nozzle heights are present. With an increase in the nozzle height, the average increase in UTS falls, thus indicating that for 1 mm nozzle height, maximum increase in the UTS is obtained. A fall in the average increase in UTS is seen for 2 mm plate thickness to 5 mm plate thickness for 2 mm nozzle height, but this can be attributed to the presence of sampling variability. The three distinct lines show a slight fall in the average increase in UTS for the 5 mm plate thickness, but the overall trend is to remain constant with a zero slope, thus indicating the absence of the main effects due to the plate thickness that can be further verified from the ANOVA results shown in Table 3. From the ANOVA results, we see the breakdown of the variability (sums of squares) of the response variable, increase in UTS. Nozzle height has the maximum contribution to the variability, and 89% of the variability in the response can be explained by the full interaction model. From

the ANOVA results we see that, for the interaction effects, the p-value (0.0694) > 0.01 (confidence level of 99%). Thus, it can be concluded that the interaction effects are negligible. Due to the absence of interaction effects, we now check for the main effects due to the plate thickness and nozzle height. The p-value for the plate thickness (t) (0.0147) > 0.01 (confidence level of 99%), thus indicating the absence of main effects due to the plate thickness. The absence of the interaction effects and main effects due to the plate thickness on the increase in UTS show that for future work the appropriate model is the additive model,

$$Y_{ijt} = \mu + \alpha_i + \varepsilon_{ijt}, \tag{2}$$

that has the assumptions that $\sum_i (\alpha)_i = 0$, where α_i are the main effects due to the nozzle height, μ is the overall mean for all treatments and ε_{ijt} is the error term.
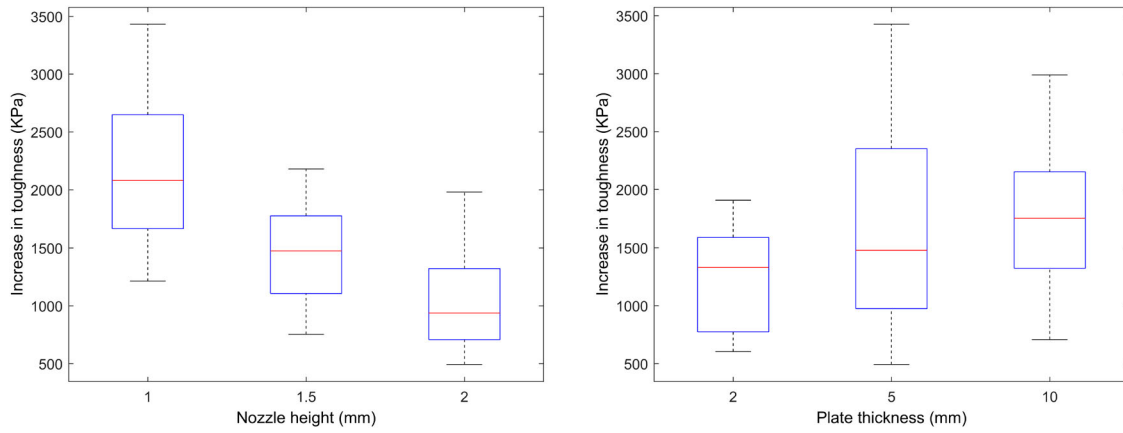
3.2.2. Increase in toughness

From the interaction plot for increase in the toughness shown in Figure 13, we see that there are three distinct lines present corresponding to the nozzle heights, indicating the presence of main effects due to the nozzle heights. Here we see that as the nozzle height increases there is a signifcant fall in the average increase in toughness of the specimen. Unlike the previously studied response (increase in the UTS) in the current response, we see an overall positive correlation of the average increase in the toughness with the plate thickness. The non-zero slopes of the lines indicate the presence of the main effects due to the plate thickness. The lines show similar trends, indicating that the interaction effects between the nozzle height and plate thickness are not important. The above inferences can be further verified from the ANOVA results obtained in Table 4.

The ANOVA results show that the nozzle height has a maximum contribution to the sums of the squares. We also see that for the interaction effects the p-value (0.1502) > 0.01 (confidence level of 99%), confirming our inference from the interaction plots that the interaction effects are not important. However, comparison of the p-values for the main effects due to the nozzle height and plate thickness show that these main effects are present for a confidence level of 99%. Due to the absence of interaction effects, for future work, an additive model is appropriate, i.e.

$$Y_{ijt} = \mu + \alpha_i + \beta_j + \varepsilon_{ijt} \tag{3}$$

with the assumptions that $\sum_i (\alpha)_i = 0$ and $\sum_j (\beta)_j = 0$, where α_i are the main effects due to nozzle height, β_j are the main effects due to plate thickness, μ is the overall mean for all treatments and ε_{ijt} is the error variable.

Figure 9. Boxplot showing the variance in the distribution of the increase in the toughness for the different nozzle heights and plate thicknesses.

3.4. Pairwise comparisons

A Tukey's pairwise comparison is carried out for both response variables to obtain the significant factor levels at a 95% confidence level. This analysis of the factor effects recognises how the factor levels are statistically different from one another. For the increase in the UTS, only the main effects due to the nozzle height are present, thus a Tukey's pairwise comparison is carried out for the different levels of the nozzle height as shown in Figure 14. The vertical lines used to connect the two factor levels are not statistically different. Figure 14 shows that all three nozzle heights have mean differences in the increase in the UTS that are statistically different from each other. This suggests that as the nozzle height is reduced from 2 mm to 1.5 mm to 1 mm progressively, higher increases in the UTS can be achieved.

For the increase in toughness, we have two main effects, namely, main effects due to the nozzle height and main effects due to the plate thickness. Figure 15 shows the line plots using Tukey's pairwise comparisons for the both the main effects. From the line plot for the nozzle heights, we see that the three levels have mean differences in the increase in the toughness that are statistically different from each other. This implies that as the nozzle height is reduced from 2 mm to 1.5 mm to 1 mm we get a progressively higher increase in the toughness. From the line plot for the plate thickness, we see that the mean differences in the increase in the toughness for the 5 and 10 mm plate are not statistically different. But we see that the 2 mm plate has mean differences which are statistically different from the 5 mm plate. This indicates that as the plate thickness is increased from 2 mm to 5 mm we see a higher increase in the toughness. But between the 5 mm plate and 10 mm plate the increase in the toughness is not significant. Thus, the maximum increase in the toughness can be achieved for the 5 mm plate or the 10 mm plate with the 1 mm nozzle height.
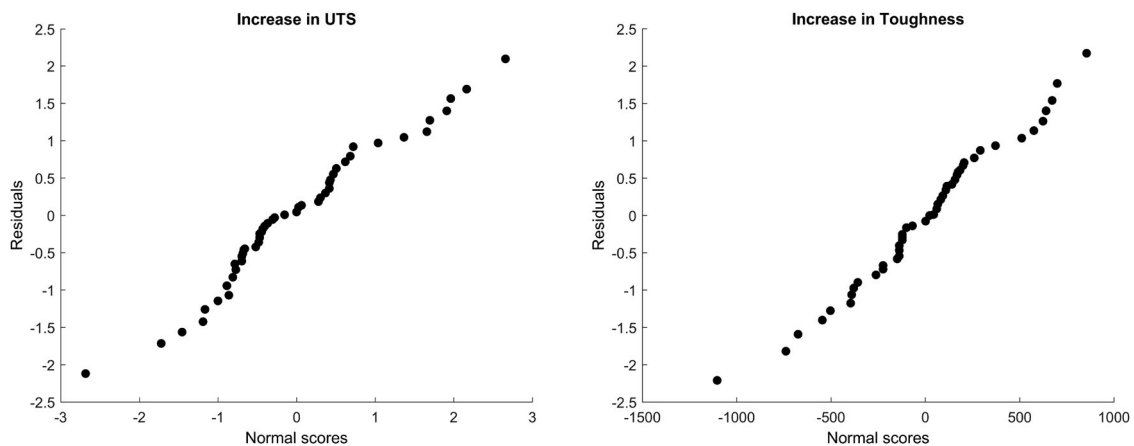
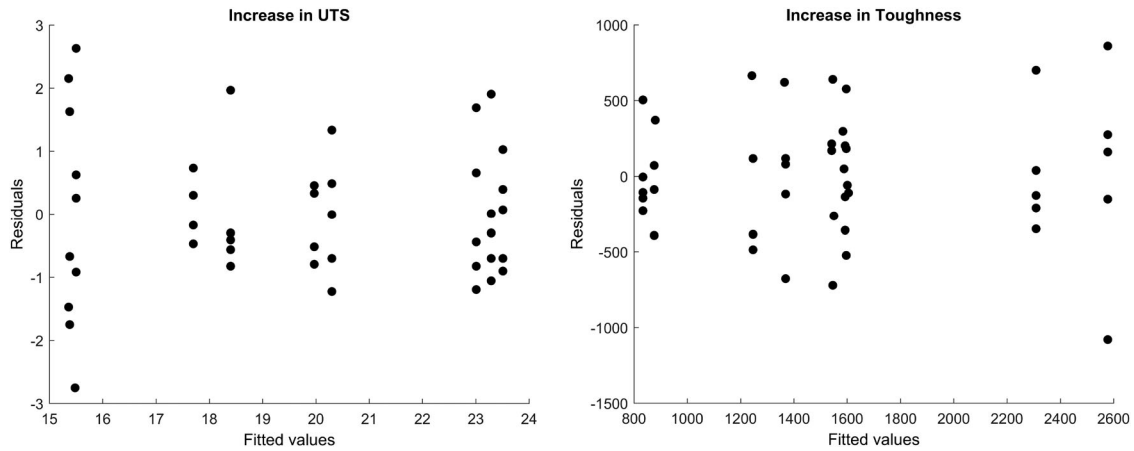**Figure 10.** Normal Probability Plot for both response variables.

Figure 11. Residuals vs. Fitted values plot.

3.5. Optimized design of heater block assembly

Based on the Tukey's pairwise comparison, it is seen that the optimised parameters for a maximum UTS and toughness are 1 mm nozzle height and 5 mm plate thickness. Based on these parameters a nozzle with an integrated plate was designed as shown in Figure 16. The 5 mm plate thickness was chosen instead of the 10 mm plate because Tukey's pairwise comparison shows that the two are not statistically different (in terms of increase in average UTS and toughness), also the 5 mm plate is lighter in weight, reducing the inertia during rapid movements due to lower mass, and it reaches the desired temperature in a shorter duration of time. Two nozzles were fabricated, one with a

25 mm plate diameter and the other with a 50 mm plate diameter. This was done to study the effect of the plate diameter on the UTS and toughness. The previous design had the heater block (with the plate) and nozzle as separate parts which were assembled as shown in Figure 16, but this caused polymer melt leakage from around the nozzle which leads to print failures and difficulty in changing a clogged nozzle. In the revised design seen in Figure 16, the plate was integrated into the nozzle thus the nozzle could be hand tightened or loosened into the heater block and reduces the assembly time if the nozzle is clogged. Five specimens were printed using each nozzle and it was seen that their effect on the UTS and the toughness
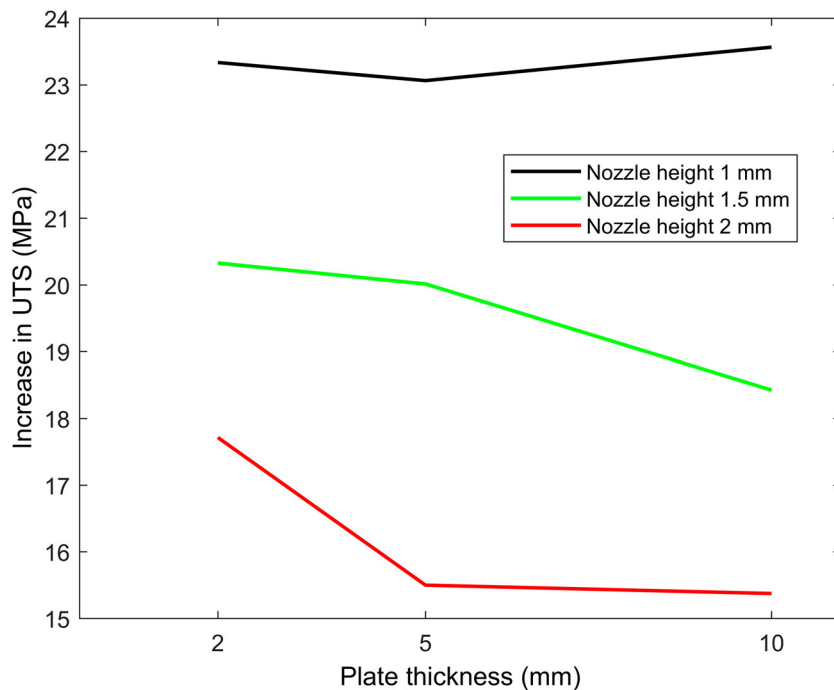

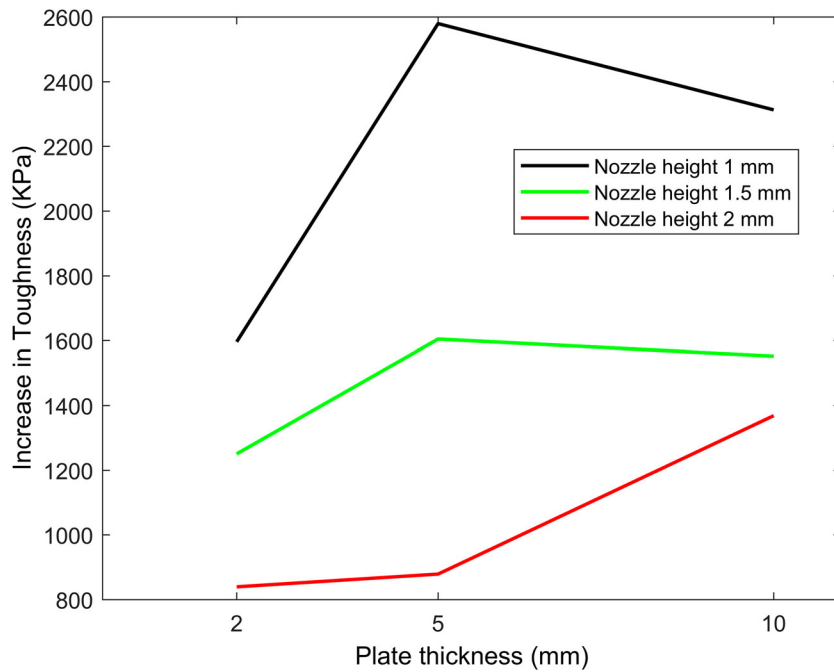**Figure 12.** Interaction plot for the increase in the UTS.

Table 3. ANOVA for the increase in UTS.

Source	Degrees of Freedom	Type III Sums of Squares	Mean Square	F value	Pr > F
Nozzle height (h)	2	378.24	189.12	129.17	<.0001
Plate thickness (t)	2	13.93	6.97	4.76	0.0147
$h \times t$	4	13.97	3.49	2.38	0.0694
Error	36	52.71	1.46		
Corrected total	44	458.85			

was similar to that of the previous design with 1 mm nozzle height and 5 mm plate thickness as seen from the stress–strain plots in Figure 17. The plate diameter does not show a significant effect on either the UTS or the toughness, this is because the printed specimens are always under the plate and are exposed to similar temperature fields for both plate diameters. Table 5 shows the increase in the average UTS and toughness for the revised design.

4. Discussion

With a change in the plate thickness, we see that the increase in the average toughness goes up as the plate becomes thicker from 2 mm to 5 mm to 10 mm. However, the Tukey's line plots suggest that the mean differences between the 5 mm plate and 10 mm plate are not statistically significant. Thus, one could choose a 5 mm plate to achieve highest average increase in the toughness. Apart from this, a 5 mm plate would be a better choice as it heats up much faster than the 10 mm plate and reduces the inertia effects in which the print head would experience greater resistance with tool path changes, hops between small distances, or even starts and stops, especially at a higher speed. The effect of greater inertia would be reflected in part quality with the potential for decreased geometric accuracy. Thus, a nozzle height of 1 mm and plate thickness of 5 mm gives us the best results for the increase in average UTS (23.2 MPa, 118.6%) and increase in average toughness (2577.4 KPa, 558.6%). The increase

Figure 13. Interaction plot for the increase in the toughness.

Table 4. ANOVA for the increase in toughness.

Source	Degrees of Freedom	Type III Sums of Squares	Mean Square	F value	Pr > F
Nozzle height (h)	2	97,36,406.44	48,68,203.2	24.65	<.0001
Plate thickness (t)	2	24,20,682.15	12,10,341.07	6.13	0.0051
$h \times t$	4	14,21,927.11	3,55,481.78	1.80	0.1502
Error	36	71,08,455.87	197,457.11		
Corrected total	44	20,687,471.57			
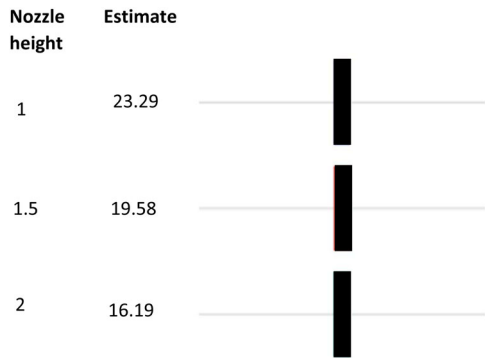
Figure 14. Line plot for Tukey's Pairwise comparison: the increase in the UTS.

in average UTS and average toughness have been summarised in Table 6 for all factor level combinations.

The increase in UTS can also be characterised by looking at the cross-sectional images as seen in Figures 18 and 19. Figure 18 shows the cross-sectional images of the failed surface for the reference and different treatment combinations. It is seen that for the reference surface, elongated voids are present between adjacent rasters. These elongated voids reduce the bond area and act as failure initiation zones leading to the low values of UTS in the reference specimens. No noticeable change in the voids is seen as the plate thickness changes from 2 mm to 10 mm, but moving from the nozzle height of 2 mm to 1 mm, the
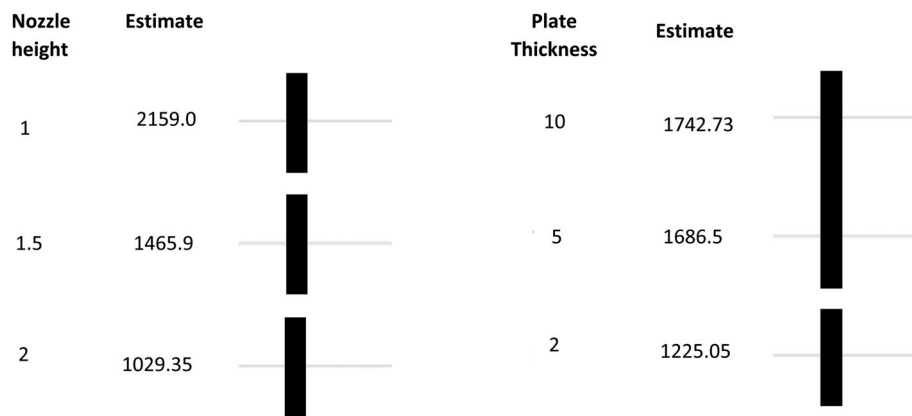
Figure 15. Line plots for Tukey's Pairwise comparison: the increase in the toughness.
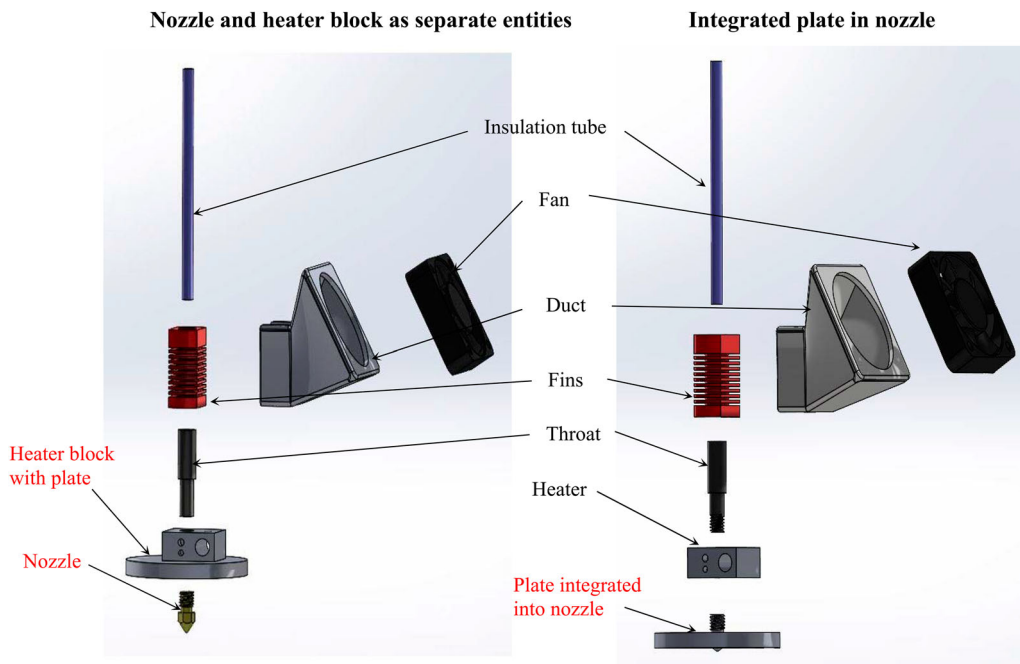
Figure 16. Optimised heater block design (on the right) as compared to the original design.
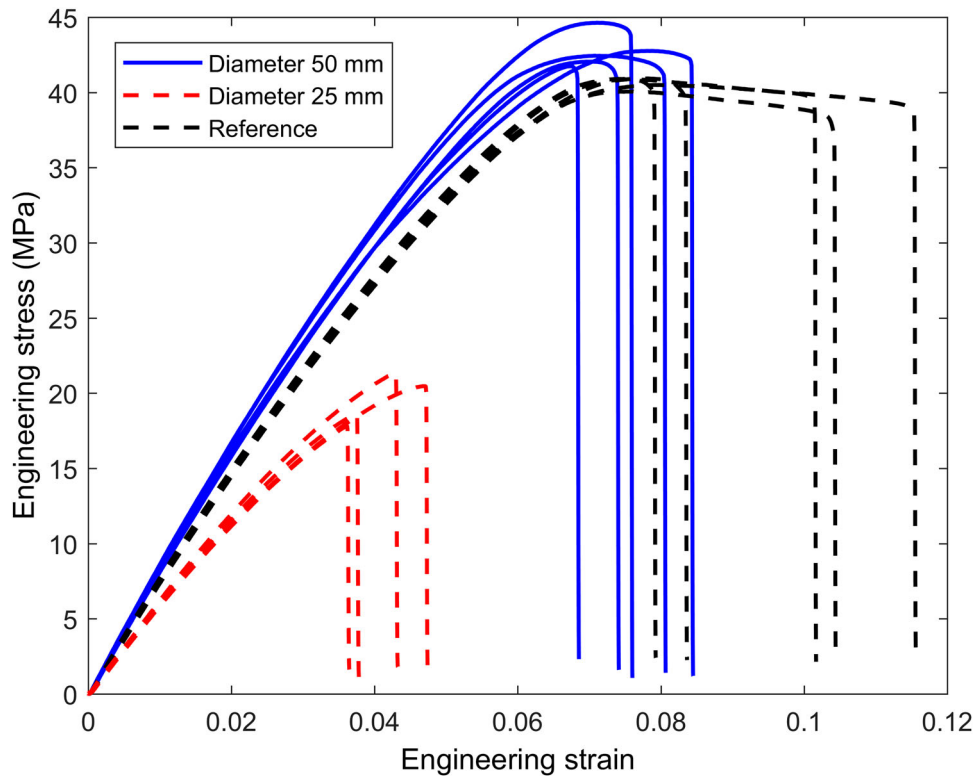
Figure 17. Stress-strain plots for specimen printed using the optimised heater block assembly.

voids coalesce together as shown in Figure 18. This leads to an increased bond area between the layers and reduces the failure initiation zones, thus increasing UTS as we reduce nozzle height to 1 mm. Also, during the testing, crazing is noticed on the parts that are printed using the modified heater block assembly, thus indicating a shift from a laminar behaviour towards homogeneity.

Figure 19 shows the changes in the void shapes and bond length for the different treatment combinations. It is seen that for the reference specimens we see equally spaced diamond shaped voids. But on studying the cross-sections of the specimen on which treatment combinations were applied, we see that the void shape changes from a diamond to a circular void. Similar changes in the void shapes have been seen in the previous studies with a post process annealing thus indicating an analogous effect that takes place here. These diamond shaped voids have sharp edges, which act as
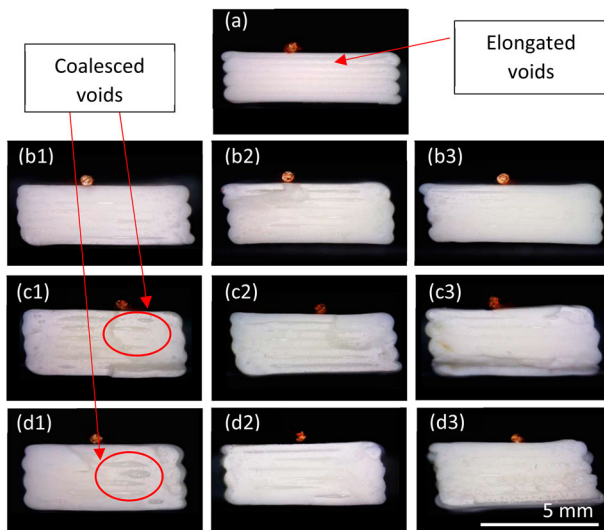
stress concentration points that cause premature failure of the reference specimen. In contrast, a shift towards circular voids reduces the stress intensity factor, thus leading to a further increase in the strength of the parts when the in-process annealing is applied. Further analyzing the images for the void area calculation through ImageJ software (Rasband, W.S., ImageJ, U. S. National Institutes of Health, Bethesda, Maryland, USA, https://imagej.nih.gov/ij/, 1997–2018) indicated that there was a slight reduction (less than 1%) in the average void area (5.56%) for the 1 mm nozzle height of all plate thicknesses in comparison to the reference specimens (6.27%). Hence the change in the void area shape has a predominant effect in comparison to the reduction in the void

Table 5. Increase in the average UTS and toughness with optimised heater block assembly.

Levels	Integrated nozzle plate diameter (mm)	Increase in average UTS (MPa)	Increase in average toughness (kPa)
1	25	24.3	2312.1
2	50	25.2	2185.2

Table 6. Increase in the average UTS and toughness for different factor level combinations.

| Levels	Plate thickness (mm)	Nozzle height (mm)	Increase in average ultimate tensile strength (MPa)	Increase in average toughness (KPa)
1	2	1.0	23.5	1591.3
2	2	1.5	20.5	1247.3
3	2	2.0	17.8	836.5
4	5	1.0	23.2	2577.4
5	5	1.5	20.1	1601.4
6	5	2.0	15.6	880.8
7	10	1.0	23.7	2308.3
8	10	1.5	18.6	1549.1
9	10	2.0	15.5	1370.7

Figure 18. (a) Cross-section of a reference coupon. (b1)–(b3) Cross-section of a coupons printed with 2 mm block with nozzle height of 1 mm, 1.5 mm and 2 mm, respectively. Similarly, (c1)–(c3) and (d1)–(d3) are representative cross-sections of specimens printed with 5 and 10 mm block with nozzle height of 1 mm, 1.5 mm and 2 mm. All cross-sections are normal to the build direction.

stiffness (increased Young's Modulus) as compared to the reference values as well as an increase in the average failure strain (0.06 or 146% for the 5 mm plate with 1 mm nozzle height). Also, the failure mode of the specimen shifts from a brittle (reference specimen) to a more elastic-brittle failure when fabricated using the modified heater block assembly. In the study, the ductility and toughness show positive correlation with each other. An increase in the ductility is seen with a decrease in the nozzle height and increase in the plate thickness. The stress–strain plots for the 5 mm plate and 10 mm plate show a similar behaviour with a noticeable brittle elastic failure at the 1 mm and 1.5 mm nozzle height. For the 2 mm plate we see an enhanced stiffness and UTS, but the failure is more brittle as compared to the other two plates.

area itself. Figure 20 shows the stress–strain plots for the different factor level combinations. The parts printed with the modified heater block assembly show enhanced

Another important inference that can be made from the stress–strain plots is that there is a change in the elastic modulus of the parts (considering only the Hookean region). For the different plate thicknesses and nozzle heights, it is seen that the increased change in the Young's modulus remains fairly constant with an average of 2144.4 ± 135.2 MPa. Table 7 shows the average Young's modulus for the reference and average Young's modulus of the parts printed using the novel print head. The increased ductility and
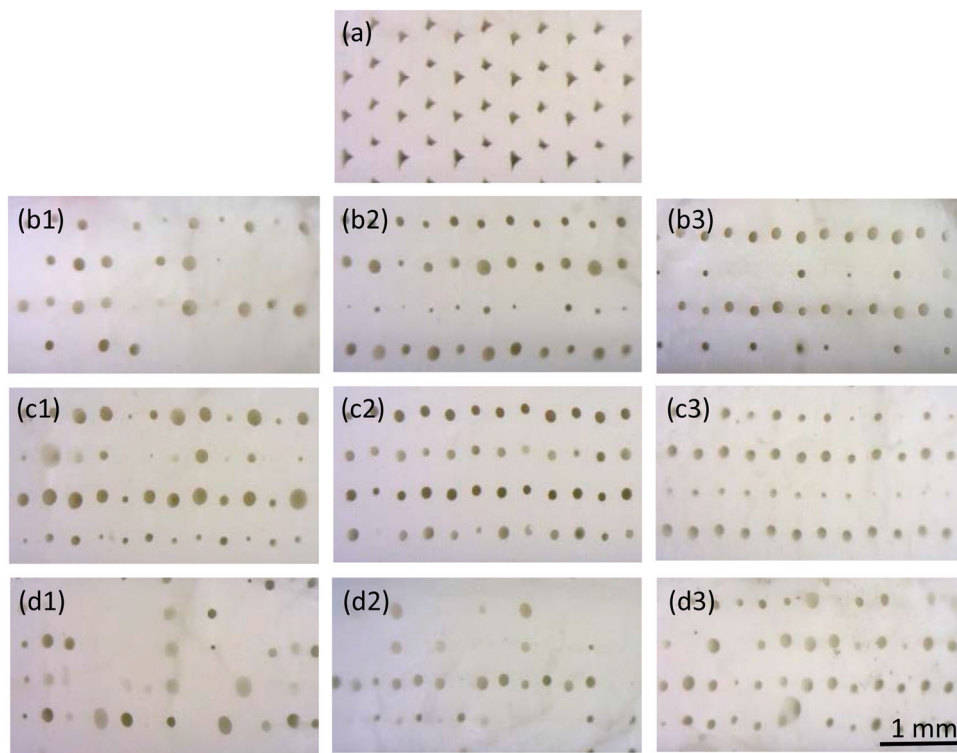
Figure 19. (a) Cross-section of a reference coupon. (b1)–(b3) Cross-section printed with 2 mm block with nozzle height of 1 mm, 1.5 mm and 2 mm, respectively. Similarly, (c1)–(c3) and (d1)–(d4) are representative cross-sections of specimens printed with 5 and 10 mm block with nozzle height of 1, 1.5 and 2 mm. All cross-sections are parallel to the build direction.
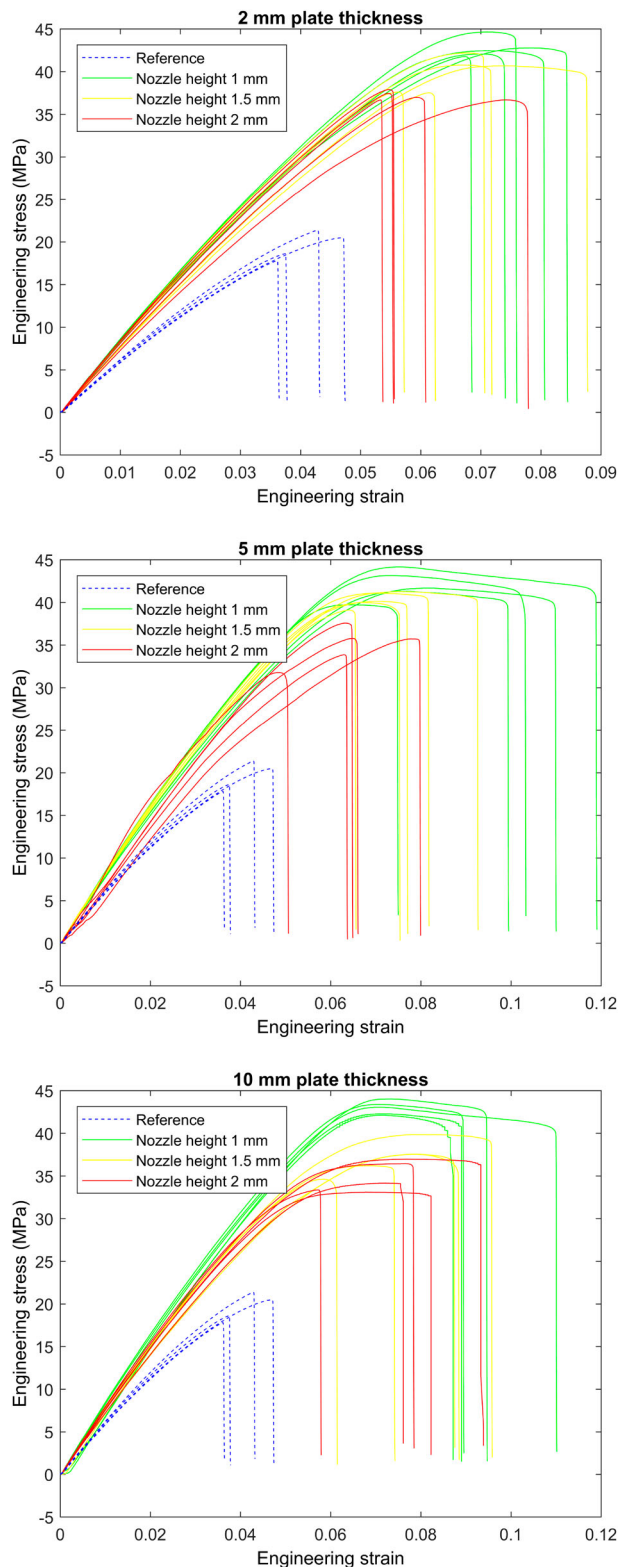
Figure 20. Stress-strain curves for specimen fabricated using different plate thicknesses and nozzle heights, and reference.

Table 7. Young's Modulus of reference and treated parts as compared with bulk material

	Young's Modulus (MPa)	Compared to bulk material
Reference	1651.8 ± 48.72	45%
Novel Print head	2144.4 ± 135.2	60%

they get excited and interact across the interface. Mobility and exchange of the polymer chain across the interface occur, which is proportional to the increase in ductility and Young's modulus. The experimental findings are thus corroborated with the reptation theory, as a higher annealing yields a higher degree of reptation and results in improved mechanical properties.

5. Conclusions

In this study, a novel modified heater block assembly was designed in an effort to improve the mechanical properties of FFF parts. A design of experiments approach was taken to characterise the effect of the nozzle height and plate thickness on the two response variables (increase in the average UTS and toughness). In the two-way, full factorial design of experiments, three factor levels were chosen for each. The specimens were tested under a tensile load to obtain the UTS and area under the stress–strain curve was calculated to calculate the toughness. The ANOVA results revealed the lack of interaction effects between the nozzle height and plate thickness for both response variables. Only main effects due to nozzle height were found to be present for the increase in UTS whereas for the increase in toughness both main effects due to the nozzle height and plate thickness were present (99% significance level). From Tukey's pairwise comparison, it is seen that the optimised factor levels for the maximum increase in the UTS and toughness are: 1 mm nozzle height and 5 mm plate thickness. For 1 mm nozzle height and 5 mm plate thickness, an increase in the average UTS of 23.2 MPa and increase in the average toughness of 2577.4 KPa was seen. Using these optimised factor levels the design was revised to now replace the separate heater block and nozzle with a single nozzle with an integrated heater plate to provide an efficient design in terms of performance and assembly time. Two diameters of nozzle integrated heater plates, 25 mm and 50 mm, were used to print 5 specimen each. These specimens showed similar behaviour to the previously studied factor level combination with the plate diameter playing no significant role as the parts being printed are always under the plate. Also, an average increase in Young's modulus by 29.8% of the specimens is

Young's modulus are associated with the higher degree of reptation. When the polymer chains are heated to a temperature above the glass transition temperature,

seen as compared to the reference when the novel print head is used. The work done in this paper provides the basis for understanding the in-process annealing process that occurs while using the novel modified heater block assembly. This work provides a relatively simple technique to improve the quality of printed parts, while solving the issues faced by the previous studies. The modified heater block assembly provides a simple and ready to use solution to improve the mechanical strength at a fraction of the cost as that of other more complicated in-process annealing designs. This paper facilitates future studies on the in-process annealing of different materials, as the same degree of in-process thermal annealing will affect differently semi-crystalline (PLA) and amorphous (ABS) polymers, and also studies involving fracture and fatigue property improvements in FFF parts.

It is important to note key limitations of the present work. While this work focuses on improved mechanical properties, the impact of in-process heating on geometrical accuracy of printed parts is also important and worthy of investigation in the future. Further, the impact of print speed of mechanical properties was not investigated here, since the print speed was always held at 60 mm/s. This was done because most PLA-related 3D printing is carried out at 60 mm/s, and therefore, the effect of changing the print speed is relatively unimportant.

Conflict of interest statement

Robert Taylor has a potential research conflict of interest due to a financial interest with Optimal Structures LLC. A management plan has been created to preserve objectivity in research in accordance with University of Texas at Arlington policy.

Notes on contributors

Parimal Patel is pursuing a PhD in Mechanical Engineering at the University of Texas at Arlington. His research interests include additive manufacturing, bio-medical product development, robotics and computer aided design, and heat transfer. He is enthusiastic about teaching and also has 3+ years of experience using additive manufacturing in bio-medical industry.

Rhugdhrivya Rane holds a PhD degree in Mechanical Engineering from the University of Texas at Arlington where his research focused on improving mechanical properties of fused filament fabricated parts.

Manjarik Mrinal holds a PhD degree in Mechanical Engineering from the University of Texas at Arlington where his research focused developing fused filament fabrication technologies to enhance mechanical properties of fused filament fabricated parts. He currently works as a researcher in HP labs.

Vishnu Ganesan is a PhD student in the Microscale Thermophysics Laboratory at University of Texas at Arlington. His research interests include heat transfer in Li-ion batteries, additive manufacturing and thermal analysis. He has published work in the past on heat transfer submodeling in Li-ion cells and powder bed modeling for additive manufacturing.

Robert Taylor is a Professor of Practice in the Mechanical and Aerospace Engineering department at the University of Texas at Arlington. Dr Taylor has a 12+ years of industry experience in general and military aircraft structural analysis with 6+ years working on F-35 structural development. His research areas are structural technology development, process informed structural design optimization for advanced manufacturing, and design for additive manufacturing.

Ankur Jain is an Associate Professor in the Mechanical and Aerospace Engineering Department at the University of Texas, Arlington. His research interests include heat transfer in Li-ion batteries, microscale thermal transport, bioheat transfer, microelectromechanical systems, etc. He has published more than 115 journal papers on these topics. He received the UT Arlington President's Award for Excellence in Teaching Award (2022), UT Arlington College of Engineering Outstanding Early Career Award (2017), NSF CAREER Award (2016) and the ASME EPP Division Young Engineer of the Year Award (2013). His research has been supported by National Science Foundation, Department of Energy, Office of Naval Research, Indo-US Science & Technology Forum and other sources.

ORCID

Ankur Jain http://orcid.org/0000-0001-5573-0674

References

Ahn, Sung Hoon, Michael Montero, Dan Odell, Shad Roundy, and Paul K. Wright. 2002. "Anisotropic Material Properties of Fused Deposition Modeling ABS." *Rapid Prototyping Journal*. doi:10.1108/13552540210441166.

Bellini, Anna, and Selçuk Güçeri. 2003. "Mechanical Characterization of Parts Fabricated Using Fused Deposition Modeling." *Rapid Prototyping Journal*. doi:10.1108/13552540310489631.

Bromberger, Jörg, and Kelly Richard. 2017. "Additive Manufacturing: A Long-Term Game Changer for Manufacturers." McKinsey & Company. Accessed April 7, 2022. https://www.mckinsey.com/business-functions/operations/our-insights/additive-manufacturing-a-long-term-game-changer-for-manufacturers.

Cole, Daniel P., Jaret C. Riddick, H. M. Iftekhar Jaim, Kenneth E. Strawhecker, and Nicole E. Zander. 2016. "Interfacial Mechanical Behavior of 3D Printed ABS." *Journal of Applied Polymer Science*. doi:10.1002/app.43671.

Compass. 2022. Accessed April 7, 2022. https://compass.astm.org/document/?contentCode=ASTM%7CD0638-14%7Cen-US&proxycl=https%3A%2F%2Fsecure.astm.org&fromLogin=true.

Costa, Ana Elisa, Alexandre Ferreira da Silva, and Olga Sousa Carneiro. 2019. "A Study on Extruded Filament Bonding in Fused Filament Fabrication." *Rapid Prototyping Journal*. doi:10.1108/RPJ-03-2018-0062.

Costa, S. F., F. M. Duarte, and J. A. Covas. 2017. "Estimation of Filament Temperature and Adhesion Development in Fused Deposition Techniques." *Journal of Materials Processing Technology*. doi:10.1016/j.jmatprotec.2017.02.026.

Dean, Angela, and Daniel Voss Springer. 2017. *Design and Analysis of Experiments*. New York: Springer Cham.

Dhal, Kashish. 2018. "On the Development and Integration of Pneumatic Extrusion Module and a Methodology to Identify Process Parameters for Additive Manufacturing Using Machine Learning."

Dimitrov, D., K. Schreve, and N. De Beer. 2006. "Advances in Three Dimensional Printing – State of the Art and Future Perspectives." *Rapid Prototyping Journal*. doi:10.1108/13552540610670717.

Domingo-Espin, Miquel, J. Antonio Travieso-Rodriguez, Ramon Jerez-Mesa, and Jordi Lluma-Fuentes. 2018. "Fatigue Performance of ABS Specimens Obtained by Fused Filament Fabrication." *Materials*. doi:10.3390/ma11122521.

Duty, Chad, Christine Ajinjeru, Vidya Kishore, Brett Compton, Nadim Hmeidat, Xun Chen, Peng Liu, Ahmed Arabi Hassen, John Lindahl, and Vlastimil Kunc. 2018. "What Makes a Material Printable? A Viscoelastic Model for Extrusion-Based 3D Printing of Polymers." *Journal of Manufacturing Processes*. doi:10.1016/j.jmapro.2018.08.008.

Gibson, Ian, David Rosen, and Brent Stucker. 2015. *Additive Manufacturing Technologies: 3D Printing, Rapid Prototyping, and Direct Digital Manufacturing, Second Edition*. doi:10.1007/978-1-4939-2113-3.

Gomez-Gras, Giovanni, Ramón Jerez-Mesa, J. Antonio Travieso-Rodriguez, and Jordi Lluma-Fuentes. 2018. "Fatigue Performance of Fused Filament Fabrication PLA Specimens." *Materials and Design*. doi:10.1016/j.matdes.2017.11.072.

Hod Lipson, Melba Kurman. 2013. *Fabricated The New World of 3D Printing*. 1st ed. Indianapolis: John Wiley&Sons, Inc.

Keleş, Özgür, Caleb Wayne Blevins, and Keith J. Bowman. 2017. "Effect of Build Orientation on the Mechanical Reliability of 3D Printed ABS." *Rapid Prototyping Journal*. doi:10.1108/RPJ-09-2015-0122.

Kopecki, Tomasz, Przemysław Mazurek, and Łukasz Święch. 2020. "The Impact of 3D Printing Parameters on the Post-Buckling Behavior of Thin-Walled Structures." *Materials*. doi:10.3390/ma13214742.

Kruth, J. P., M. C. Leu, and T. Nakagawa. 1998. "Progress in Additive Manufacturing and Rapid Prototyping." *CIRP Annals - Manufacturing Technology*. doi:10.1016/S0007-8506(07)63240-5.

Lanzotti, Antonio, Marzio Grasso, Gabriele Staiano, and Massimo Martorelli. 2008. "Effect of Processing Conditions on the Bonding Quality of FDM Polymer Filaments." *Rapid Prototyping Journal*.

Ligon, Samuel Clark, Robert Liska, Jürgen Stampfl, Matthias Gurr, and Rolf Mülhaupt. 2017. "Polymers for 3D Printing and Customized Additive Manufacturing." *Chemical Reviews*. doi:10.1021/acs.chemrev.7b00074.

Luo, Cheng, Manjarik Mrinal, Xiang Wang, and Ye Hong. 2021. "Bonding Widths of Deposited Polymer Strands in Additive

Manufacturing." *Materials* 14(4), 871. Multidisciplinary Digital Publishing Institute. doi:10.3390/MA14040871.

Osborn, T., E. Zhou, R. Gerzeski, D. Mollenhauer, G. P. Tandon, T. J. Whitney, and E. V. Iarve. 2015. "Experimental and Theoretical Evaluation of Stiffness Properties of Fused Deposition Modeling Parts." In *Proceedings of the American Society for Composites – 30th Technical Conference, ACS 2015*.

Patel, P. T. 2018. "Additive Manufacturing Process Investigation for the Fabrication of Composite Scaffolds for Soft Tissue Application." https://search.proquest.com/openview/104f1fb261b9dcf371af1f394d255270/1?pq-origsite=gscholar&cbl=18750&diss=y.

Patel, Parimal T., Prashanth Ravi, Panos S. Shiakolas, Tré R. Welch, and Tushar Saini. 2019. "Additive Manufacturing of Heterogeneous Bio-Resorbable Constructs for Soft Tissue Applications." In *Materials Science and Technology 2018, MS and T 2018*. doi:10.7449/2018/MST_2018_1496_1503.

Percoco, Gianluca, Fulvio Lavecchia, and Luigi Maria Galantucci. 2012. "Compressive Properties of FDM Rapid Prototypes Treated with a Low Cost Chemical Finishing." *Research Journal of Applied Sciences, Engineering and Technology* 4 (19): 3838–3842.

Pham, D. T., and R. S. Gault. 1998. "A Comparison of Rapid Prototyping Technologies." *International Journal of Machine Tools and Manufacture*. doi:10.1016/S0890-6955(97)00137-5.

Puigoriol-Forcada, Josep M., Alex Alsina, Antonio G. Salazar-Martín, Giovanni Gomez-Gras, and Marco A. Pérez. 2018. "Flexural Fatigue Properties of Polycarbonate Fused-Deposition Modelling Specimens." *Materials and Design*. doi:10.1016/j.matdes.2018.06.018.

Rane, Rhugdhrivya. 2018. "Enhancing Tensile Strength of FDM Parts Using Thermal Annealing and Uniaxial Pressure" Accessed April 7, 2022. https://www.proquest.com/docview/2201931722/87429CAF67714E44PQ/1?accountid=7117

Rane, Rhugdhrivya, Akhilesh Kulkarni, Hardikkumar Prajapati, Robert Taylor, Ankur Jain, and Victoria Chen. 2020. "Post-Process Effects of Isothermal Annealing and Initially Applied Static Uniaxial Loading on the Ultimate Tensile Strength of Fused Filament Fabrication Parts." *Materials*. doi:10.3390/ma13020352.

Ravoori, Darshan, Hardikkumar Prajapati, Viswajit Talluru, Ashfaq Adnan, and Ankur Jain. 2019. "Nozzle-Integrated Pre-Deposition and Post-Deposition Heating of Previously Deposited Layers in Polymer Extrusion Based Additive Manufacturing." *Additive Manufacturing*. doi:10.1016/j.addma.2019.06.006.

Rodriguez, Jose F., James P. Thomas, and John E. Renaud. 2000. "Characterization of the Mesostructure of Fused-Deposition Acrylonitrile-Butadiene-Styrene Materials." *Rapid Prototyping Journal*. doi:10.1108/13552540010337056.

Rodríguez, José F., James P. Thomas, and John E. Renaud. 2001. "Mechanical Behavior of Acrylonitrile Butadiene Styrene (ABS) Fused Deposition Materials. Experimental Investigation." *Rapid Prototyping Journal*. doi:10.1108/13552540110395547.

Skawiński, Igor, and Tomasz Goetzendorf-Grabowski. 2019. "FDM 3D Printing Method Utility Assessment in Small RC Aircraft Design." *Aircraft Engineering and Aerospace Technology*. doi:10.1108/AEAT-07-2018-0189.

Sood, Anoop K., Raj K. Ohdar, and Siba S. Mahapatra. 2012. "Experimental Investigation and Empirical Modelling of

FDM Process for Compressive Strength Improvement." *Journal of Advanced Research*. doi:10.1016/j.jare.2011.05.001.

Sweeney, Charles B., Blake A. Lackey, Martin J. Pospisil, Thomas C. Achee, Victoria K. Hicks, Aaron G. Moran, Blake R. Teipel, Mohammad A. Saed, and Micah J. Green. 2017. "Welding of 3D-Printed Carbon Nanotube–Polymer Composites by Locally Induced Microwave Heating." *Science Advances*. doi:10.1126/sciadv.1700262.

Tamburrino, F., S. Barone, A. Paoli, and A. V. Razionale. 2021. "Post-Processing Treatments to Enhance Additively Manufactured Polymeric Parts: A Review." *Virtual and Physical Prototyping*. doi:10.1080/17452759.2021.1917039.

Taylor, Robert M., Nicholas Lira, Gavin Sabine, Joakim Lea, Craig Conklin, Bijan Niakan, and Sangram Advirkar. 2020. "Design Optimization, Fabrication, and Testing of a 3d Printed Aircraft Structure Using Fused Deposition Modeling." In *AIAA Scitech 2020 Forum*. doi:10.2514/6.2020-1924.

Tolochko, Nikolay K., Maxim K. Arshinov, Andrey V. Gusarov, Victor I. Titov, Tahar Laoui, and Ludo Froyen. 2003. "Mechanisms of Selective Laser Sintering and Heat Transfer in Ti Powder." *Rapid Prototyping Journal*. doi:10.1108/13552540310502211.

Turner, Brian N., Robert Strong, and Scott A. Gold. 2014. "A Review of Melt Extrusion Additive Manufacturing Processes: I. Process Design and Modeling." *Rapid Prototyping Journal*. doi:10.1108/RPJ-01-2013-0012.

Wong, Kaufui V., and Aldo Hernandez. 2012. "A Review of Additive Manufacturing." *ISRN Mechanical Engineering*. doi:10.5402/2012/208760.

Zaldivar, R. J., D. B. Witkin, T. McLouth, D. N. Patel, K. Schmitt, and J. P. Nokes. 2017. "Influence of Processing and Orientation Print Effects on the Mechanical and Thermal Behavior of 3D-Printed ULTEM ® 9085 Material." *Additive Manufacturing*. doi:10.1016/j.addma.2016.11.007.

Zein, Iwan, Dietmar W. Hutmacher, Kim Cheng Tan, and Swee Hin Teoh. 2002. "Fused Deposition Modeling of Novel Scaffold Architectures for Tissue Engineering Applications." *Biomaterials*. doi:10.1016/S0142-9612(01)00232-0.

Zhang, Baicheng, Hanlin Liao, and Christian Coddet. 2012. "Effects of Processing Parameters on Properties of Selective Laser Melting Mg-9%Al Powder Mixture." *Materials and Design*. doi:10.1016/j.matdes.2011.06.061.

Ziemian, Sophia, Maryvivian Okwara, and Constance Wilkens Ziemian. 2015. "Tensile and Fatigue Behavior of Layered Acrylonitrile Butadiene Styrene." *Rapid Prototyping Journal*. doi:10.1108/RPJ-09-2013-0086.